

Current-driven mechanical motion of double stranded DNA results in structural instabilities and chiral-induced-spin-selectivity of electron transport

Nicholas S. Davis

College of Science and Engineering, James Cook University, Townsville, QLD, 4811, Australia

Julian A. Lawn

College of Science and Engineering, James Cook University, Townsville, QLD, 4811, Australia

Riley J. Preston

Institute of Physics, University of Freiburg, Hermann-Herder-Strasse 3, 79104 Freiburg, Germany

Daniel S. Kosov

College of Science and Engineering, James Cook University, Townsville, QLD, 4811, Australia

Chiral-induced-spin-selectivity of electron transport and its interplay with DNA's mechanical motion is explored in a double stranded DNA helix with spin-orbit-coupling. The mechanical degree of freedom is treated as a stochastic classical variable experiencing fluctuations and dissipation induced by the environment as well as force exerted by nonequilibrium, current-carrying electrons. Electronic degrees of freedom are described quantum mechanically using nonequilibrium Green's functions. Nonequilibrium Green's functions are computed along the trajectory for the classical variable taking into account dynamical, velocity dependent corrections. This mixed quantum-classical approach enables calculations of time-dependent spin-resolved currents. We showed that the electronic force may significantly modify the classical potential which, at sufficient voltage, creates a bi-stable potential with considerable effect on electronic transport. The DNA's mechanical motion has a profound effect on spin transport; it results in chiral-induced spin selectivity increasing spin polarisation of the current by 9% and also resulting in temperature-dependent current voltage characteristics. We demonstrate that the current noise measurement provides an accessible experimental means to monitor the emergence of mechanical instability in DNA motion. The spin resolved current noise also provides important dynamical information about the interplay between vibrational and spin degrees of freedom in DNA.

I. INTRODUCTION

Chiral-induced-spin-selectivity (CISS) is an intriguing phenomenon observed in a wide range of molecules and conditions [1–4]. Primarily this effect pertains to the preferential spin current flowing in each direction across the molecule, attracting interest in biochemistry due to the link between spin currents and enantioselectivity [5] and controlling reactions [6, 7] as well as spintronics [8–13] due to the magnitude of spin-polarisation (SP) [14]. This significant SP is surprising given the weak spin-orbit-coupling (SOC) in organic molecules[15], and many avenues have been explored to reconcile the difference between experimental observation and theoretical prediction. Consequently, the emergence of a large SP has been attributed to many different effects, yet a definitive description of CISS remains elusive.

Measurements of the CISS effect have continued since its discovery in attempts to elucidate its underlying mechanisms. This has led to a few key observations that warrant consideration when designing effective models. The first is that the magnitude of SP increases with the length of the molecule[16–18], indicating a compounding mechanism as electrons traverse the molecule. Also apparent is the sensitivity of SP to temperature[19]; sparking a strong interest in vibrational effects.

It has been well established that there is no spin

separability in a system involving only a single transport channel. Time-reversibility of SOC allows its removal via a gauge transformation; thus spin cannot separate[11, 20, 21]. In junctions with single-point contact to only two leads, it is necessary for the molecule itself to possess multiple spin-transport channels, which is the case for double-stranded DNA with inter-strand exchange. Furthermore, it has been demonstrated that while a two-terminal setup using a ferromagnet is sufficient to detect CISS effects in a non-linear transport regime [22], a multi-terminal setup is necessary for the linear response regime [11].

Beyond attempts to magnify the SOC within the molecule [23–25], several aspects of molecular transport have featured prominently as candidates for core functions of CISS. Many models neglect electron-electron interactions, yet their inclusion has proved to greatly enhance SP [26, 27]. A similar case holds for electron-phonon interactions when including nuclear vibrations [16, 28]. Furthermore, these effects are necessary to include as the single-electron treatment cannot fully describe CISS [29, 30].

The importance of nuclear vibrations to CISS is expanded upon here, where we consider DNA's mechanical motion coupled to electronic degrees of freedom. The mechanical motion is considered classically, in which it evolves in time under the influence of the force pro-

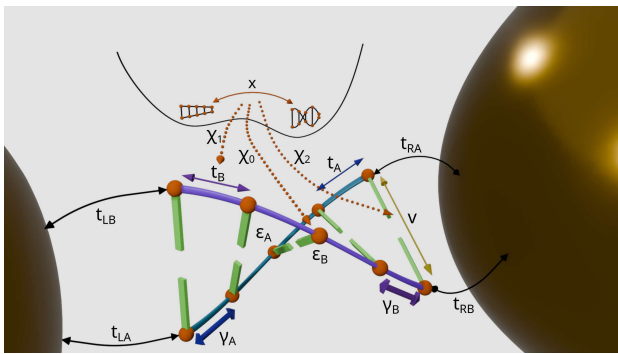


FIG. 1: Schematic of the model system. Double stranded DNA connects two electrodes. The DNA's mechanical motion influences the on-site energies, intra-strand electronic hopping, and inter-strand electron transfer. γ_A and γ_B denote SOC, which is included in our model as spin-dependent intra-strand coupling. Both strands of DNA are attached to the electrodes.

duced by nonequilibrium quantum electrons. Inherently advantageous to this approach is the versatility of the mechanical coordinate, which can experience large amplitude motion in complex potential energy landscapes. The dynamics of DNA's mechanical motion is modelled using a Langevin equation with nonequilibrium electronic forces computed via nonequilibrium Green's functions (NEGF). These calculations of time-dependent current include non-adiabatic dynamical corrections arising from the time-dependence of the electronic Hamiltonian which depends parametrically on the mechanical variable. Aside from the SP, which is the topic of most studies, this approach facilitates the calculation of spin-resolved current noise, where dynamical corrections arising due to a breakdown of the Born-Oppenheimer approximation play an important role.

The paper is organised as follows. Section II describes the theory; the model Hamiltonian, NEGF calculations of current and forces, and the numerical scheme to solve the Langevin equation with NEGF forces. Results are presented and discussed in Section III, focusing on the average nonequilibrium energy landscape for DNA's mechanical motion, along with current and current noise induced by DNA's mechanical motion. Section IV presents the conclusions.

We use atomic units in our equations: $\hbar = e = 1$. Most values of physical quantities will also be stated in atomic units (a.u.); however, we will present the values for all energy related quantities in eV and voltages in V, for clarity.

II. THEORY

A. Model

The system consists of a double-stranded DNA molecule with the ends linked to two macroscopic electrodes. Each nucleotide in the DNA is represented as a single electronic level. The electrons are allowed to hop within a single strand between neighbouring nucleotides as well as between nucleotides within the base pair. The electronic Hamiltonian depends on the DNA conformation, for which the nuclear dynamics are collectively described by a single mechanical degree of freedom.

The system is described by the Hamiltonian

$$H(t) = H_M + H_L + H_R + H_{ML} + H_{MR} + H_{e\text{-mech}}(x) + H_{\text{mech}}(p, x), \quad (1)$$

which is partitioned into the DNA Hamiltonian H_M , left and right electrodes $H_L + H_R$, the electronic coupling of the DNA to the electrodes $H_{ML} + H_{MR}$, the coupling of tunneling electrons to the mechanical degree of freedom $H_{e\text{-mech}}$, and, finally, the mechanical degree of freedom $H_{\text{mech}}(p, x)$. The electronic Hamiltonian is time-dependent through the dependence on the mechanical degree of freedom $x(t)$. The electrodes' Hamiltonians take the form of non-interacting electronic reservoirs:

$$H_L + H_R = \sum_{\alpha k \sigma} \epsilon_{\alpha k \sigma} d_{\alpha k \sigma}^\dagger d_{\alpha k \sigma}, \quad (2)$$

where d^\dagger and d are the standard creation and annihilation operators and the subscript $\alpha k \sigma$ denotes the action of the operator in electrode $\alpha \in \{L, R\}$ on single-particle state k with spin $\sigma \in \{\uparrow, \downarrow\}$. A visualisation of our proposed molecular junction configuration is shown in Fig. 1.

The molecular Hamiltonian describes a double-stranded DNA helix with spin-orbit-coupling, as in Refs. [31, 32]:

$$H_M = \sum_{\beta j \sigma} \epsilon_\beta d_{\beta j \sigma}^\dagger d_{\beta j \sigma} + \sum_{\beta j \sigma} t_\beta (d_{\beta j \sigma}^\dagger d_{\beta, j+1, \sigma} + \text{h.c.}) + \sum_{j \sigma} v (d_{A j \sigma}^\dagger d_{B j \sigma} + \text{h.c.}) + V_{\text{SOC}}. \quad (3)$$

Here, subscript j is the base-pair index for strand $\beta \in \{A, B\}$, ϵ_β is the on-site energy, while t_β and v are the intra-chain and inter-chain hopping matrix elements, respectively. These hopping integrals are treated as equal for all sites within each strand. However, the strands are assumed to be different. As such, adopting parameters similar to Refs. [32]: $\epsilon_A = -0.2$ eV, $\epsilon_B = 0.1$ eV, $t_A = 0.1$ eV, $t_B = -0.14$ eV and $v = -0.08$ eV.

The spin-orbit coupling (SOC) is

$$V_{\text{SOC}} = \sum_{\beta j \sigma \sigma'} i \gamma_\beta \Lambda_{\sigma \sigma'}^{\beta j} d_{\beta j \sigma}^\dagger d_{\beta, j+1, \sigma'} + \text{h.c.} \quad (4)$$

The SOC matrix $\Lambda_{\sigma\sigma'}^{\beta j}$ contains constants determined by the geometry of the helix, defined by helix angle θ and rotation per base pair ϕ ,

$$\Lambda_{\uparrow\uparrow}^{\beta j} = 2 \cos \theta, \quad \Lambda_{\downarrow\downarrow}^{\beta j} = -2 \cos \theta, \quad (5)$$

$$\Lambda_{\uparrow\downarrow}^{\beta j} = i(-)_{\beta}(e^{-i\phi(j-1)} + e^{-i\phi j}) \sin \theta, \quad \Lambda_{\downarrow\uparrow}^{\beta j} = \left(\Lambda_{\uparrow\downarrow}^{\beta j}\right)^*, \quad (6)$$

where $(-)_{\beta}$ is $(+1)$ if $\beta = A$ and (-1) if $\beta = B$. The SOC strength constants are taken as $\gamma_A = -0.014$ eV and $\gamma_B = 0.01$ eV, similar to [32].

The mechanical degree of freedom (x, p) is described by a Hamiltonian for a classical particle of mass m

$$H_{\text{mech}}(x) = \frac{p^2}{2m} + U(x), \quad (7)$$

with harmonic potential $U(x) = \frac{1}{2}m\omega_0 x^2$. This frequency is chosen within a range to reflect the vibrational dynamics of DNA, with standard value $\omega_0 = 5$ meV [33]. Finally, the mass, $m = 5.9244 \times 10^5$ a.u., is taken as the approximate mass of a single nucleotide. Quantum effects become important, and the classical treatment of nuclear dynamics generally fails, when the temperature is smaller than the characteristic frequency of nuclear motion. In this paper, we perform our calculations at $T = 300$ K (25.8 meV) and $T = 77$ K (6.6 meV), where both temperatures are above the frequency of the DNA's mechanical motion, ω_0 , considered in our model. Therefore, we expect that our classical approach provides a qualitatively correct description given our focus on the low energy mechanical motion of DNA and relatively high temperatures.

The interaction between electrons and the mechanical degree of freedom is assumed to be described by linear response to the classical coordinate x , and is given by

$$\begin{aligned} H_{\text{e-mech}}(x) = & -\chi_0 \sqrt{2m\omega_0} x \sum_{\beta j \sigma} d_{\beta j \sigma}^{\dagger} d_{\beta j \sigma} \\ & - \chi_1 \sqrt{2m\omega_0} x \sum_{\beta j \sigma} (d_{\beta j \sigma}^{\dagger} d_{\beta, j+1, \sigma} + \text{h.c.}) \\ & - \chi_2 \sqrt{2m\omega_0} x \sum_{j \sigma} (d_{A j \sigma}^{\dagger} d_{B j \sigma} + \text{h.c.}) \end{aligned} \quad (8)$$

Here, the first term describes the on-site electron-mechanical motion interaction, the second term takes into account the influence of the mechanical motion on the intra-strand electronic hopping, and the last term deals with inter-strand electron transfer assisted by the mechanical motion of DNA. The corresponding coupling strengths are described by χ_0 , χ_1 and χ_2 . Following Refs. [32, 34, 35], we assume that $\chi_1 = 0.2\chi_0$, $\chi_2 = \chi_1$. The value of χ_0 will be treated as a parameter to study the role of the strength of the electron-vibration coupling on the results.

The system-electrode coupling is described by

$$H_{ML} = \sum_{k\beta\sigma} \left(t_{Lk,\beta 1} d_{Lk\sigma}^{\dagger} d_{\beta 1\sigma} + \text{h.c.} \right), \quad (9)$$

$$H_{MR} = \sum_{k\beta\sigma} \left(t_{Rk,\beta N} d_{Rk\sigma}^{\dagger} d_{\beta N\sigma} + \text{h.c.} \right), \quad (10)$$

where $t_{\alpha k, \beta 1}$ and $t_{\alpha k, \beta N}$ are the tunnelling amplitudes between electrodes' states $\alpha k \sigma$ and corresponding DNA base-pair 1 or N for left and right couplings, respectively. Thus, it is assumed that both strands of DNA are attached to the electrodes.

B. Green's Functions with nonadiabatic corrections

The self-energies and Green's functions are matrices in molecular spin-orbital space with dimension $(2 \times 2 \times N)$, where N is the number of base-pairs in the DNA, 2 is for the number of DNA strands and another 2 for the spin degrees of freedom.

We treat self-energies in the wide-band approximation, within which the matrix elements of the retarded component are

$$\Sigma_{L,\beta j \sigma, \beta' j' \sigma'}^R = -\frac{i}{2} \Gamma_L \delta_{\beta \beta'} \delta_{j 1} \delta_{j' 1} \delta_{\sigma \sigma'}, \quad (11)$$

$$\Sigma_{R,\beta j \sigma, \beta' j' \sigma'}^R = -\frac{i}{2} \Gamma_R \delta_{\beta \beta'} \delta_{j N} \delta_{j' N} \delta_{\sigma \sigma'}, \quad (12)$$

where Γ_{α} is the level broadening function due to the coupling to electrode α . The advanced self energy matrices are obtained via the Hermitian conjugate of the retarded components

$$\Sigma_{\alpha}^A = (\Sigma_{\alpha}^R)^{\dagger}. \quad (13)$$

Finally, the lesser self-energies are computed via the fluctuation-dissipation relation as

$$\Sigma_{\alpha}^<(\omega) = f_{\alpha}(\omega) (\Sigma_{\alpha}^A - \Sigma_{\alpha}^R), \quad (14)$$

where

$$f_{\alpha}(\omega) = \frac{1}{1 + e^{(\omega - \mu_{\alpha})/k_B T}}, \quad (15)$$

is the Fermi-Dirac occupation number for electrode α with chemical potential μ_{α} and temperature T . In all calculations we assume the the voltage V is applied symmetrically: $\mu_L = V/2$ and $\mu_R = -V/2$.

Suppose we know a trajectory $(x(t), p(t))$ for the mechanical degree of freedom. The electronic part of the Hamiltonian in Eq. (1) becomes explicitly time-dependent through the parametric dependence on $x(t)$, which means that the Green's functions should be obtained from the solution of the full Keldysh-Kadanoff-Baym equations. Following Refs. [36–38], we use a time-separation technique to solve the Keldysh-Kadanoff-Baym equations in the Wigner space, resulting in the expression

$$\mathbf{G}(t, \omega) = \mathbf{G}_{(0)}(t, \omega) + \mathbf{G}_{(1)}(t, \omega). \quad (16)$$

Here ,

$$\mathbf{G}(t, \omega) = \int d(t_1 - t_2) e^{i\omega(t_1 - t_2)} \mathbf{G}(t_1, t_2), \quad (17)$$

is the Wigner space Green's function and $t = (t_1 + t_2)/2$ is the central time. $\mathbf{G}_{(0)}(t, \omega)$ is the adiabatic Green's function (Green's function which instantaneously follows the changes in the reaction coordinate) and $\mathbf{G}_{(1)}(t, \omega)$ contains non-adiabatic corrections (accounting for the dynamics of mechanical motion). The adiabatic Green's functions are the standard Green's functions computed for a static Hamiltonian. The advanced and retarded Green's functions are computed by matrix inversion

$$\mathbf{G}_{(0)}^{A/R}(t, \omega) = \left(\omega - \mathbf{h}(x(t)) - \Sigma^{A/R} \right)^{-1}, \quad (18)$$

where the matrix \mathbf{h} is formed from the electronic Hamiltonian including the coupling to the mechanical motion term:

$$\begin{aligned} h_{\beta j \sigma, \beta' j' \sigma'} &= (\epsilon_\beta - \chi_0 \sqrt{2m\omega_0 x}) \delta_{\beta\beta'} \delta_{jj'} \delta_{\sigma\sigma'} \\ &+ (t_\beta - \chi_1 \sqrt{2m\omega_0 x}) \delta_{\beta\beta'} \delta_{j\pm 1, j'} \delta_{\sigma\sigma'} \\ &+ (v - \chi_2 \sqrt{2m\omega_0 x}) (1 - \delta_{\beta\beta'}) \delta_{jj'} \delta_{\sigma\sigma'} \\ &+ i\Lambda_{\sigma\sigma'}^{\beta j} \gamma_\beta \delta_{\beta\beta'} \delta_{j\pm 1, j'}. \end{aligned} \quad (19)$$

The lesser adiabatic Green's function is computed using advanced and retarded components

$$\mathbf{G}_{(0)}^<(t, \omega) = \mathbf{G}_{(0)}^R(t, \omega) \Sigma^<(\omega) \mathbf{G}_{(0)}^A(t, \omega). \quad (20)$$

The first order nonadiabatic corrections to the advanced and retarded Green's functions are (functional dependence on t and ω is suppressed for brevity)

$$\mathbf{G}_{(1)}^{A/R} = \frac{1}{2i} \mathbf{G}_{(0)}^{A/R} \left[\mathbf{G}_{(0)}^{A/R}, \dot{\mathbf{h}} \right]_- \mathbf{G}_{(0)}^{A/R}, \quad (21)$$

where $\dot{\mathbf{h}}$ is the time derivative of matrix (19)

$$\begin{aligned} \dot{h}_{\beta j \sigma, \beta' j' \sigma'} &= -\dot{x} \sqrt{2m\omega_0} \delta_{\sigma\sigma'} \left(\chi_0 \delta_{\beta\beta'} \delta_{jj'} \right. \\ &\left. + \chi_1 \delta_{\beta\beta'} \delta_{j\pm 1, j'} + \chi_2 (1 - \delta_{\beta\beta'}) \delta_{jj'} \right). \end{aligned} \quad (22)$$

The nonadiabatic correction to the lesser component is

$$\begin{aligned} \mathbf{G}_{(1)}^< &= \mathbf{G}_{(0)}^{A/R} \Sigma^< \mathbf{G}_{(1)}^A + \mathbf{G}_{(1)}^R \Sigma^< \mathbf{G}_{(0)}^A \\ &+ \frac{1}{2i} \mathbf{G}_{(0)}^R \left(\dot{\mathbf{h}} \mathbf{G}_{(0)}^R \partial_\omega \Sigma^< + \mathbf{G}_{(0)}^< \dot{\mathbf{h}} + \text{h.c.} \right) \mathbf{G}_{(0)}^A. \end{aligned} \quad (23)$$

C. Spin-resolved current with dynamical corrections and force exerted by electrons on mechanical degree of freedom

Spin resolved electronic current, which includes dynamical corrections due to the mechanical motion, is

obtained as in Refs. [36–39]. The adiabatic current (depends on instantaneous position $x(t)$) is given by the standard expression

$$\begin{aligned} J_{\alpha\sigma}^{(0)}(t) &= \int_{-\infty}^{\infty} \frac{d\omega}{2\pi} \text{Tr} \left[\mathbf{G}_{(0)}^< \Sigma_{\alpha\sigma}^A + \mathbf{G}_{(0)}^R \Sigma_{\alpha\sigma}^< \right. \\ &\quad \left. - \Sigma_{\alpha\sigma}^< \mathbf{G}_{(0)}^A - \Sigma_{\alpha\sigma}^R \mathbf{G}_{(0)}^< \right], \end{aligned} \quad (24)$$

while the first order correction is given by

$$\begin{aligned} J_{\alpha\sigma}^{(1)}(t) &= \int_{-\infty}^{\infty} \frac{d\omega}{2\pi} \text{Tr} \left[\mathbf{G}_{(1)}^< \Sigma_{\alpha\sigma}^A \right. \\ &\quad \left. + \mathbf{G}_{(1)}^R \Sigma_{\alpha\sigma}^< - \Sigma_{\alpha\sigma}^< \mathbf{G}_{(1)}^A - \Sigma_{\alpha\sigma}^R \mathbf{G}_{(1)}^< \right. \\ &\quad \left. + \frac{1}{2i} \left(\dot{\mathbf{G}}_{(0)}^R \partial_\omega \Sigma_{\alpha\sigma}^< + \partial_\omega \Sigma_{\alpha\sigma}^< \dot{\mathbf{G}}_{(0)}^A \right) \right], \end{aligned} \quad (25)$$

where

$$\dot{\mathbf{G}}_{(0)}^A = \mathbf{G}_{(0)}^A \dot{\mathbf{h}} \mathbf{G}_{(0)}^A, \quad (26)$$

$$\dot{\mathbf{G}}_{(0)}^R = \left(\dot{\mathbf{G}}_{(0)}^A \right)^\dagger, \quad (27)$$

and the derivative $\partial_\omega \Sigma_{\alpha\sigma}^<$ can be easily computed using the wide-band approximation expression for $\Sigma_{\alpha\sigma}^<$.

We turn our attention now to calculations of the force exerted by nonequilibrium electrons on the mechanical degree of freedom. The force operator is computed by differentiating the corresponding part of the electronic Hamiltonian

$$\begin{aligned} \hat{F}_e(t) &= -\partial_x H_{e\text{-mech}}(t) \\ &= - \sum_{\beta j \sigma, \beta' j' \sigma'} (\partial_x h)_{\beta j \sigma, \beta' j' \sigma'} d_{\beta j \sigma}^\dagger d_{\beta' j' \sigma'}, \end{aligned} \quad (28)$$

where

$$\begin{aligned} (\partial_x h)_{\beta j \sigma, \beta' j' \sigma'} &= -\sqrt{2m\omega_0} \delta_{\sigma\sigma'} \left(\chi_0 \delta_{\beta\beta'} \delta_{jj'} \right. \\ &\quad \left. + \chi_1 \delta_{\beta\beta'} \delta_{j\pm 1, j'} + \chi_2 (1 - \delta_{\beta\beta'}) \delta_{jj'} \right). \end{aligned} \quad (29)$$

Taking a quantum average along with truncation due to a time-scale separation yields

$$F_e(t) = i \int \frac{d\omega}{2\pi} \text{Tr} \left[\partial_x \mathbf{h} \mathbf{G}_{(0)}^<(t, \omega) \right]. \quad (30)$$

This force can then be integrated over x and added to the classical potential to produce an effective potential for the classical coordinate produced by nonequilibrium current-carrying electrons.

D. Dynamics of the mechanical degree freedom

The mechanical degree of freedom x is treated as a stochastic classical variable experiencing fluctuations and dissipation induced by the environment as well as force exerted by nonequilibrium, current carrying electrons. To simulate the effect of the environment, the equation of motion of the mechanical coordinate is defined by a Langevin equation,

$$p = m\dot{x}, \quad (31)$$

$$\dot{p}(t) = f(t) - \zeta(t)p + \eta(t), \quad (32)$$

where the force

$$f(t) = -m\omega_0^2 x + F_{e,\text{neq}}(t), \quad (33)$$

contains a classical oscillator term with spring constant $m\omega_0^2$, and a nonequilibrium electronic force $F_{e,\text{neq}}$. The nonequilibrium electronic force is defined as

$$F_{e,\text{neq}} = F_e(x) - F_{e,\text{eq}}(x), \quad (34)$$

where the electronic force F_e is given by (30) and $F_{e,\text{eq}}(x)$ is the equilibrium electronic force computed at zero voltage bias. This equilibrium force removal is justified based on the assumption that the equilibrium potential energy surface is completely represented by the harmonic potential term $\frac{1}{2}m\omega_0^2 x^2$. The environment terms, viscosity ζ and white noise random force $\eta(t)$ are related to each other by the fluctuation dissipation theorem $\langle \eta(t)\eta(t') \rangle = m\zeta kT \delta(t-t')$.

To integrate the Langevin equation (31,32) we use the BAOAB splitting algorithm[40]. The algorithm breaks up the Langevin equation into three separate finite difference equations: Inertial momentum update (B), position update (A) and a momentum update due to the stochastic force (O); it involves NEGF calculations of force on each internal momentum update step (B). This algorithm has been shown to be more accurate in comparison to other Langevin integrators, particularly being very robust to changes in time-step; it also provides accurate barrier crossing times for 1D double-welled potentials [40] which is important for bistable DNA's mechanical motion considered in our paper. We use integration time-step 1 a.u. and viscosity $\zeta = 2.228 \times 10^{-4}$ a.u. in all our simulations.

III. RESULTS

A. Electronic current induces mechanical instability

We begin by examining the effective potential energy experienced by the mechanical degree of freedom

$$U(x) = \frac{1}{2}m\omega_0^2 x^2 - \int_{x_0}^x dx F_{e,\text{neq}}(x), \quad (35)$$

where the electronic force $F_{e,\text{neq}}$ is given by Eq. (30) and choice of x_0 is arbitrary.

The inclusion of the nonequilibrium electronically-induced force on the x coordinate is observed to introduce a double-well potential feature to the ordinarily harmonic oscillator for some parameters. Firstly, considering high temperature (300 K), it is observed that for low voltages $V < 0.11$ V the effective potential is roughly parabolic with a single potential minimum. As the voltage is increased the effective potential widens and a centralised energy barrier U_B emerges separating two minima. As can be seen in Figures 2(a),(b),(c), this change is gradual and initially the barrier is below the thermal energy with respect to the lowest minima, ($U_B < k_B T$), but for higher voltages $V > 0.17$ V it is above ($U_B > k_B T$). This behaviour continues up to $V = 0.34$ V, after which the barrier begins to subside. The qualitatively similar behaviour is observed at $T = 77$ K, although the low temperature ensures that the barrier, once present, always exceeds thermal energy; shown in Figures 2(b),(d),(f). The influence of the nonequilibrium electronic force is more pronounced at low temperature – additional minima start to develop at smaller voltage and the minima are separated by higher potential barriers.

The parameter space is further explored at $T = 300$ K in Figure 3 where the shaded regions indicate the qualitative nature of the potential resulting from the strength of electron-mechanical-motion coupling χ_0 and voltage V . At the relatively low voltages considered, the molecular electronic population tends to increase with voltage, and so does the electronic force (30). This force is due to the electron-mechanical motion interaction, so χ_0 also scales the magnitude and thus both parameters contribute to the development of double-minima potential. In addition to the distinction between single well and double well potentials, Figure 3 also emphasises the distinction between the double-potential when the barrier is above and below the thermal energy. Results presented in 2(a),(b), and (c) correspond to points A, B, C in Figure 3. We use $\chi_0 = 0.0316$ eV in all our calculations for the rest of the paper.

To understand the dynamics of DNA's mechanical motion in a bistable potential, it is instructive to view occupation probabilities for left and right minima. For this, we perform Langevin simulations by numerically solving Eqs. (31, 32) at $T = 300$ K and $T = 77$ K. These occupation probabilities are defined as $P_\alpha = \tau_\alpha / \tau_{\text{total}}$, where τ_α is the time which the mechanical coordinate spends in potential side $\alpha = L, R$ during the total trajectory time τ_{total} . As can be seen from the occupation of the left and right minima in Figure 4, in the room temperature regime ($T = 300$ K), the occupation probability of the left minima is not substantially suppressed even when the barrier exceeds the thermal energy. Thermal fluctuations allow the coordinate to overcome the barrier. In the lower temperature regime ($T = 77$ K), the leftmost minima is "frozen out" of the dynamics leading to an effectively zero occupation when the barrier energy

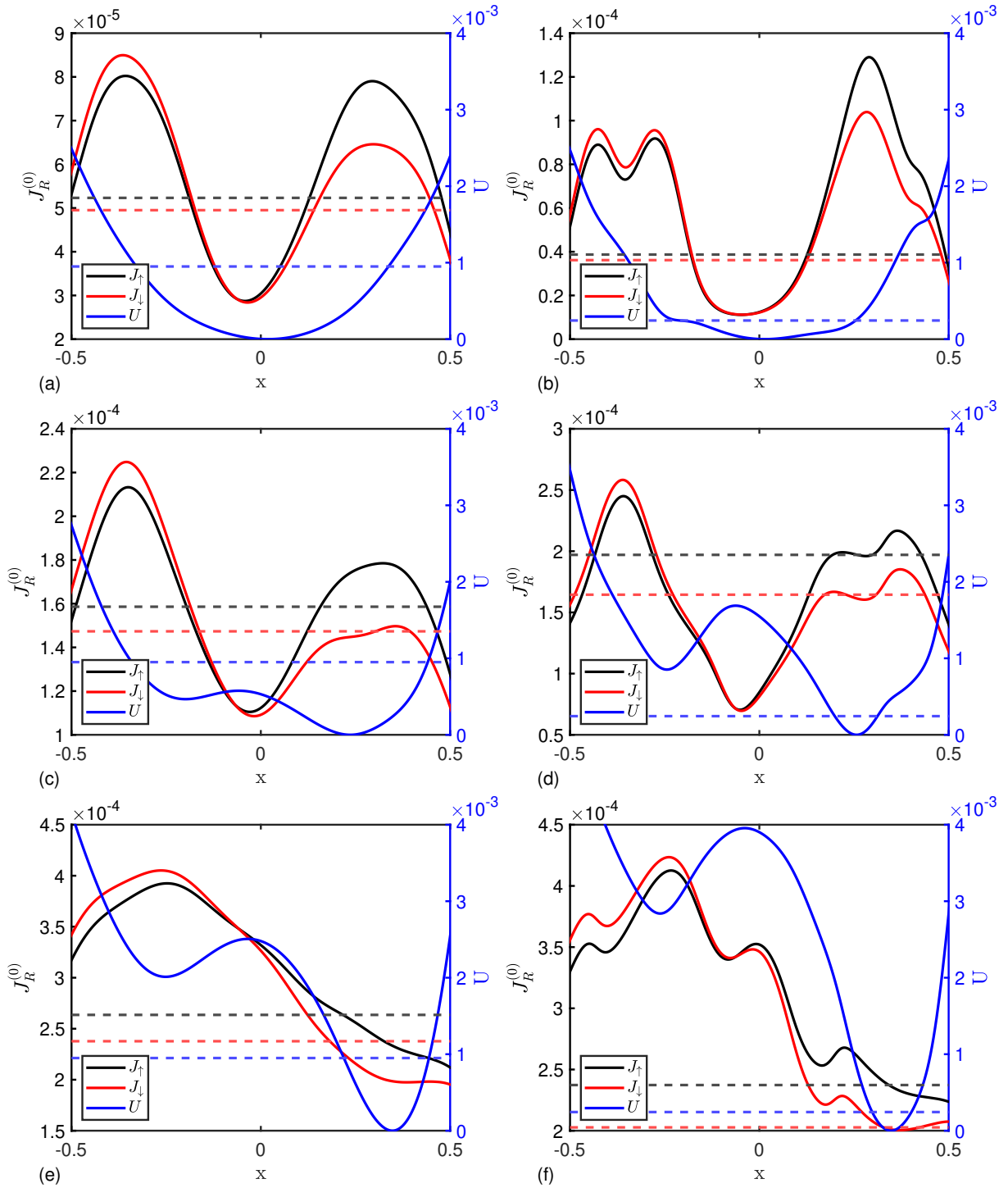


FIG. 2: Left-side axis: Spin-resolved current profile for adiabatic current $J_{R\sigma}^{(0)}(x)$. Dashed horizontal lines indicate mean current values computed via averaging over values of the current over Langevin trajectory. Right-side axis: Total potential $U(x)$. Dashed horizontal line indicates thermal energy above minimum. Voltages shown: 0.05 V (a-b), 0.14 V (c-d), 0.29 V (e-f). $T = 300$ K (left column) and $T = 77$ K (right column), $\chi_0 = 0.0361$ eV.

is sufficiently above the temperature.

B. Mechanical motion induces spin-polarisation of electronic current

Figure 2(a)-(f) shows a nontrivial dependence of the spin-resolved electric currents on the mechanical coordi-

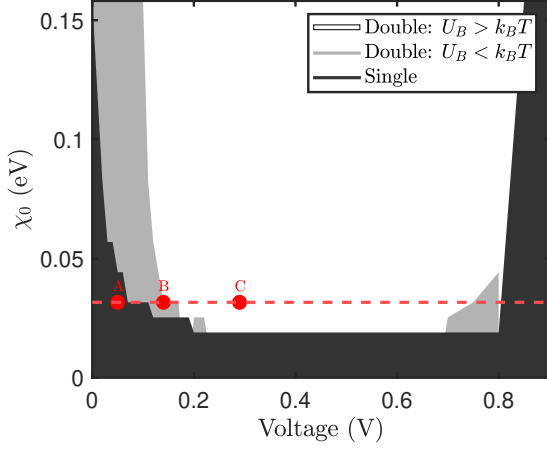


FIG. 3: System parameter map indicating the nature of the effective potential $U(x)$ (35) for the combination of electron-mechanical motion strength χ_0 and voltage V . The potential is defined by the number of local minima: either a single or double potential well and, for the double potential, whether the barrier between minima is greater than the thermal energy. Point A, B, and C correspond to voltages 0.05 V, 0.14 V, and 0.29 V, respectively. Dashed line represents $\chi_0 = 0.0316$ eV. $T = 300$ K.

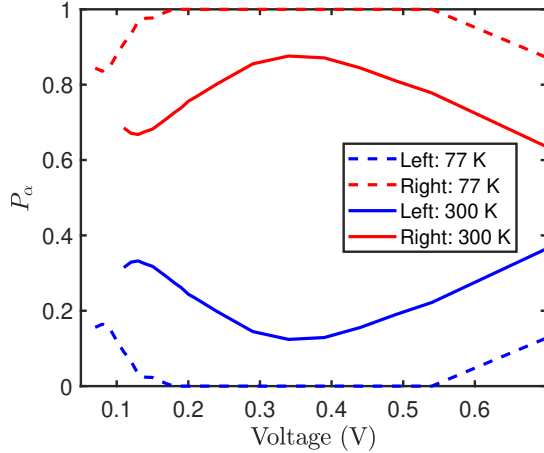


FIG. 4: Occupation probability for each left/right region of double potential in blue/red, respectively, computed at temperatures $T = 300$ K and $T = 77$ K.

nate x . The metastable left minima, which is populated more at higher temperatures, corresponds to more conductive DNA junctions – the electronic current is larger for both spin components here in comparison to the stable right minima. These differences in electronic currents for stable and metastable DNA configurations are reflected in the current-voltage characteristics shown in Figure 5. As one can see in Figure 5, the electronic current computed at $T = 300$ K is larger than the current

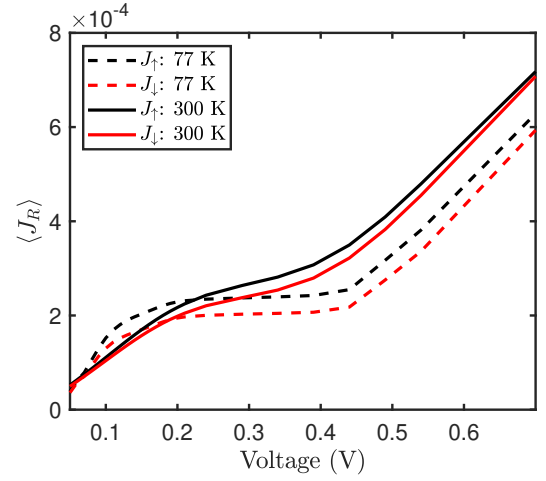


FIG. 5: Time-averaged spin currents computed at $T = 300$ K and $T = 77$ K as a function of voltage.

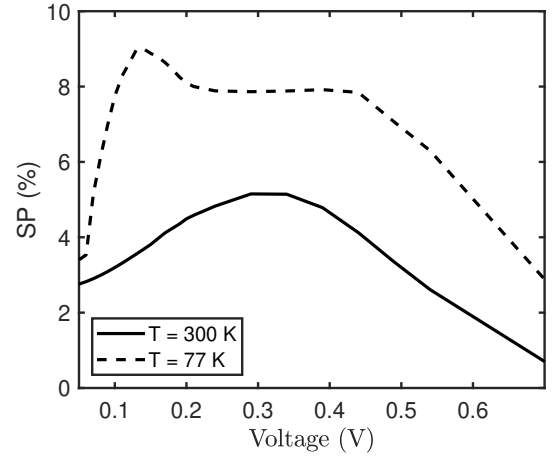


FIG. 6: Spin polarisation, $SP = (J_{\uparrow} - J_{\downarrow}) / (J_{\uparrow} + J_{\downarrow})$, computed at $T = 300$ K and $T = 77$ K as a function of voltage.

at $T = 77$ K; this observation is qualitatively consistent with the experimental data [27]. Note that there is no noticeable temperature dependence of the electronic current in the absence of coupling between the DNA's mechanical motion and the electronic degrees of freedom.

Figure 2(a)-(f) also shows that the DNA's mechanical motion in the stable (right) potential induces considerable majority-spin polarisation of the current whereas metastable DNA configuration favours minority-spin to a lesser extent. Given that high temperature enables greater access to the left region, the time-averaged current will receive greater contribution to minority-spin current. As a result, the spin polarisation of electronic current decreases with increasing temperature as one can see from Figure 6. For $T = 300$ K, spin-polarisation increases from roughly 2-5% and is maximised at 0.3 V. Beyond this the spin polarisation reduces with voltage.

Meanwhile for $T = 77$ K, spin-polarisation increases from 3-9% up to 0.2 V. SP maintains up to 0.4 V then also decays at high voltage. This temperature dependence is contrary to the aforementioned experiment [27] – we delegate this problem to future study.

C. Spin-resolved current noise assisted by DNA's mechanical motion

Being a time-averaged quantity, the current-voltage characteristic (Figure 5) does not provide information about the DNA dynamics; it does not reveal the important time-scales related to the effective potential shapes. To reveal experimentally accessible information about DNA's mechanical motion and its interplay with spin polarisation, we turn our attention to spin-resolved current noise calculations. Note also that the dynamical (velocity dependent) corrections to the electric current do not play any role so far, since their contributions disappear upon averaging over trajectory due to being linear in the velocity. However, the corrections play a role in the current noise.

Noise spectroscopy in molecular junctions has proven useful in identifying transport mechanisms not discernible from the current-voltage characteristics alone. Such measurements can reveal atomistic details of the local environment and metal-molecule interfaces [41, 42], coupling between electronic and vibrational degrees of freedom [43–47], individual conduction transport channels [48–51], and mechanical stability of the junction [52]. Naturally, extending these ideas to consider spin noise provides insight into spin transport. Indeed, shot noise has been used to identify spin-polarised transport within a specific spin channel [53]. Spin fluctuations can reveal Rabi splittings, Zeeman shifts, and the formation of doublet and triplet states [54]; also enabling disturbance-free probing of spin dynamics [55, 56]. Shot noise calculations [57, 58] have explored contributions to quantum noise and its correlations; however the role of molecular, mechanical motion is largely unexplored. In what follows, we quantify the noise as a result of this motion.

The spin-resolved current noise is formally defined as

$$S_{\alpha,\sigma\sigma'}(\tau) = \lim_{T \rightarrow +\infty} \frac{1}{T} \int_0^T dt \langle [\delta\hat{J}_{\alpha\sigma}(t), \delta\hat{J}_{\alpha\sigma}(t+\tau)]_+ \rangle, \quad (36)$$

where $\delta\hat{J}_{\alpha\sigma}(t)$ describes the instantaneous deviation of the σ -spin current at time t from its mean value and $[\dots]_+$ is the anti-commutator. The quantum expectation value $\langle \dots \rangle$ averages over electronic degrees of freedom while the time average over the mechanical motion of DNA is described by $\lim_{T \rightarrow +\infty} \frac{1}{T} \int_0^T dt \dots$; equivalent to an ensemble average of DNA geometries. This total noise is a complex amalgamation of various sources of noise. Quantum noise is inherent to electrons due to discrete charge, Pauli exclusion principle, shot noise, finite temperature and the correlations arising from electron-

electron interactions. The latter is excluded from our model of non-interacting electrons. Additionally, a mechanical noise results from the current-induced motion of the DNA. Due to the time-scale separation of electrons and this molecular motion, this contribution from the noise can be isolated [59]. The characteristic time scale of shot noise decay is $1/\Gamma$, whereas the noise due to nuclear motion appears on much longer times, $1/\zeta$. For the viscosity considered, $\zeta/\Gamma \approx 0.006$; hence the noise induced by geometrical fluctuations dominates the noise power spectrum at low frequencies, and can exceed the shot noise contribution by orders of magnitude. In what follows we focus on the “mechanical” noise as

$$S_{\alpha,\sigma\sigma'}(\tau) = 2 \lim_{T \rightarrow +\infty} \frac{1}{T} \int_0^T dt \delta J_{\alpha\sigma}(t+\tau) \delta J_{\alpha\sigma'}(t), \quad (37)$$

where the current fluctuation at time t is

$$\delta J_{\alpha\sigma}(t) = J_{\alpha\sigma}(t) - \lim_{T \rightarrow +\infty} \frac{1}{T} \int_0^T dt J_{\alpha\sigma}(t). \quad (38)$$

The adiabatic mechanical noise

$$S_{\alpha,\sigma\sigma'}^{(0)}(\tau) = 2 \lim_{T \rightarrow +\infty} \frac{1}{T} \int_0^T dt \delta J_{\alpha\sigma}^{(0)}(t+\tau) \delta J_{\alpha\sigma'}^{(0)}(t), \quad (39)$$

and dynamical corrections, which not only depend on the instantaneous position but also on the velocity,

$$S_{\alpha,\sigma\sigma'}^{(1)}(\tau) = 2 \lim_{T \rightarrow +\infty} \frac{1}{T} \int_0^T dt \left[\dot{x}(t+\tau) B_{\alpha\sigma}(t+\tau) \delta J_{\alpha\sigma'}^{(0)}(t) + \delta J_{\alpha\sigma}^{(0)}(t+\tau) \dot{x}(t) B_{\alpha\sigma'}(t) + \dot{x}(t+\tau) B_{\alpha\sigma}(t+\tau) \dot{x}(t) B_{\alpha\sigma'}(t) \right], \quad (40)$$

are included in the total noise

$$S_{\alpha,\sigma\sigma'}(\tau) = S_{\alpha,\sigma\sigma'}^{(0)}(\tau) + S_{\alpha,\sigma\sigma'}^{(1)}(\tau). \quad (41)$$

Here we factorised the dynamical correction to the electric current

$$J_{\alpha\sigma}^{(1)}(t) = \dot{x} B_{\alpha\sigma}(x). \quad (42)$$

As we will demonstrate, the terms (39), (40) are responsible for different features of noise correlation functions. The adiabatic mechanical noise $S_{\alpha,\sigma\sigma'}^{(0)}(\tau)$ is generally featureless and shows overall exponential decay. The first two cross correlation terms in $S_{\alpha,\sigma\sigma'}^{(1)}(\tau)$ (the terms which are linear in velocity of mechanical motion) are responsible for the deviation of $S_{\alpha,\uparrow\downarrow}(\tau)$ from $S_{\alpha,\downarrow\uparrow}(\tau)$ for bistable mechanical motion. The last term in $S_{\alpha,\sigma\sigma'}^{(1)}(\tau)$ involves velocity-velocity correlations containing the underlying dip and peak features at half-period and full-period of motion in the right region.

Figures 7 (a,b) show spin resolved components of current noise for DNA's mechanical motion in single-potential shown in Figure 2-a. Adiabatic mechanical

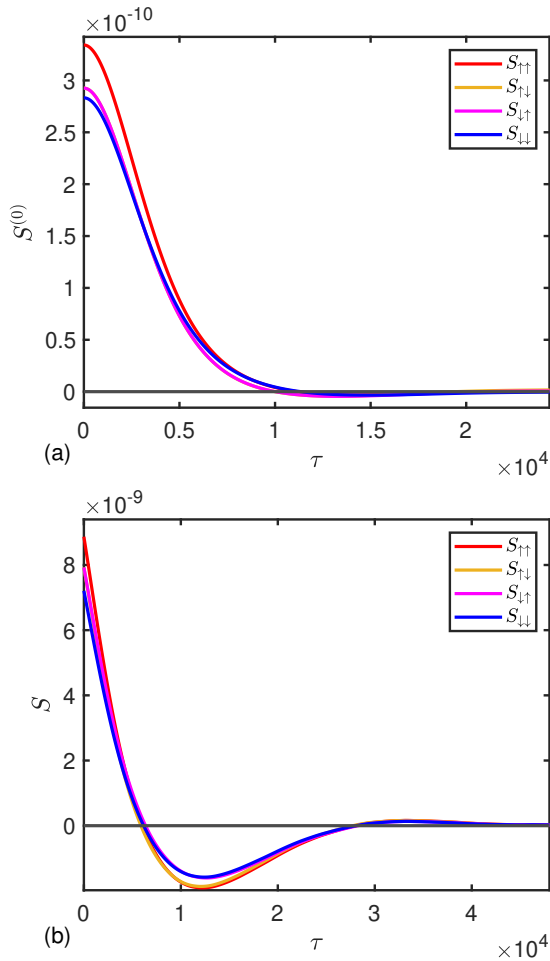


FIG. 7: Spin-resolved noise $S_{R,\sigma\sigma'}(\tau)$ for single-minima effective potential (corresponds to point A in Figure 3). (a) Adiabatic noise (39), (b) total noise computed with dynamical corrections (41).

noise $S^{(0)}(\tau)$ demonstrates simple decay of correlations in time with no distinct features. Once dynamical corrections are included, the noise reveals negative correlations at times comparable to the half-period - this dip is a characteristic feature of classical velocity-velocity correlation functions and, unsurprisingly, it can be shown that it originates predominantly from the last term in Eq. (40) which contains $\dot{x}(t + \tau)\dot{x}(t)$.

Figures 8 (a,b) show the spin resolved components of current noise for DNA bistable mechanical motion shown in Figure 2-e. Adiabatic noise $S^{(0)}(\tau)$ remains always positive and begins to develop small positive-correlation features, due to the consistently large deviation of the current from its average value for stable (right) potential and at the same time consistently smaller current dispersion in metastable (left) potential - see 2-e. Dynamically corrected noise reveals a distinct negative contribution to correlations (dip) at approximately the half-period of mechanical motion in the stable potential and a positive-correlation (peak) appears at approximately of full period

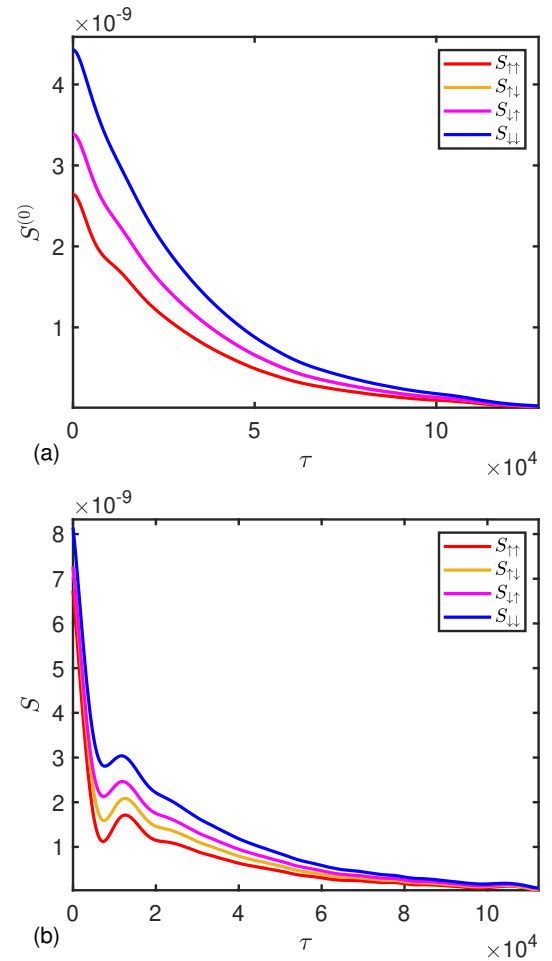


FIG. 8: Spin-resolved noise $S_{R,\sigma\sigma'}(\tau)$ for bistable mechanical motion (corresponds to point C in Figure 3). a) Adiabatic noise (39), (b) total noise computed with dynamical corrections (41).

of above motion - this feature again takes its origin from the velocity-velocity correlation term in Eq. (40). It is interesting to note that although the average current is dominated by $\sigma = \uparrow$ electrons - see Figure 6, the noise shows the opposite spin selectivity: $S_{\alpha,\uparrow\uparrow}(\tau)$ is always smaller than $S_{\alpha,\downarrow\downarrow}(\tau)$ due to smaller deviation of $J_{\alpha\uparrow}(x)$ from the mean compared to $J_{\alpha\downarrow}(x)$.

The interesting new feature associated with mechanical bistability is the different temporal correlations between fluctuations of spin-up and spin-down currents depending upon which fluctuations occurred first - as it is apparent from Figure 8 (b), cross-spin noise $S_{\alpha,\uparrow\downarrow}(\tau)$ deviates from $S_{\alpha,\downarrow\uparrow}(\tau)$. Analysis of the sum of two terms in current noise dynamical corrections, $\dot{x}(t + \tau)B_{\alpha\sigma}(t + \tau)\delta J_{\alpha\sigma'}^{(0)}(t)$ and $\delta J_{\alpha\sigma'}^{(0)}(t + \tau)\dot{x}(t)B_{\alpha\sigma'}(t)$ shows that the up-down component is negative whereas the down-up component is positive (at the timescale of noise correlation decay).

IV. CONCLUSIONS

We have explored mechanical motion due to current induced forces in a double stranded DNA helix with spin-orbit-coupling and its role in the spin polarisation of current and noise induced by DNA chirality. We represent the mechanical motion according to the dynamics of a stochastic classical variable experiencing fluctuations and dissipation induced by the environment as well as forces exerted by nonequilibrium, current carrying electrons. The electronic degrees of freedom are described quantum mechanically using NEGF. NEGF are computed along the trajectory for the classical variable taking into account dynamical, velocity dependent corrections.

We observe that

- DNA's mechanical instability is induced by tunneling electrons. The instability emerges at moderate applied voltage bias given that the strength of electron-mechanical motion coupling exceeds a certain critical value. The physical regimes for stable and bistable DNA motion are identified.
- Mechanical motion results in moderate increase of

SP, achieving 3-9% depending on the temperature and voltage bias. This is compared to the absence of any SP without mechanical motion. The comparatively small SP is expected given the short helix.

- The temperature-dependent energy landscape together with temperature-dependent dynamics of the mechanical motion lead to considerable temperature dependence of the electronic current. The temperature dependence of the total current agrees with experimental observation, however, SP does not show the expected response to increased temperature. This raises questions about the importance of additional interactions such as allowing the mechanical motion to flip the spin via SOC mechanisms which are not included in the present study.
- The spin resolved noise induced by DNA's mechanical motion can be a useful experimental tool to extract information about DNA mechanical motion and detect the emergence of mechanical instabilities.

-
- [1] C. D. Aiello, J. M. Abendroth, M. Abbas, A. Afanasev, S. Agarwal, A. S. Banerjee, D. N. Beratan, J. N. Belling, B. Berche, A. Botana, J. R. Caram, G. L. Celardo, G. Cuniberti, A. Garcia-Etxarri, A. Dianat, I. Diez-Perez, Y. Guo, R. Gutierrez, C. Herrmann, J. Hihath, S. Kale, P. Kurian, Y.-C. Lai, T. Liu, A. Lopez, E. Medina, V. Mujica, R. Naaman, M. Noormandipour, J. L. Palma, Y. Paltiel, W. Petuskey, J. C. Ribeiro-Silva, J. J. Saenz, E. J. G. Santos, M. Solyanik-Gorgone, V. J. Sorger, D. M. Stemer, J. M. Ugalde, A. Valdes-Curiel, S. Varela, D. H. Waldeck, M. R. Wasielewski, P. S. Weiss, H. Zacharias, and Q. H. Wang, "A chirality-based quantum leap," *ACS Nano*, vol. 16, no. 4, pp. 4989–5035, 2022.
- [2] R. Naaman, Y. Paltiel, and D. Waldeck, "Chiral molecules and the electron spin," *Nat Rev Chem*, vol. 3, pp. 250–260, 2019.
- [3] R. Naaman, Y. Paltiel, and D. H. Waldeck, "Chiral induced spin selectivity gives a new twist on spin-control in chemistry," *Accounts of Chemical Research*, vol. 53, no. 11, pp. 2659–2667, 2020.
- [4] R. Naaman and D. H. Waldeck, "Spintronics and chirality: Spin selectivity in electron transport through chiral molecules," *Annual Review of Physical Chemistry*, vol. 66, no. 1, pp. 263–281, 2015.
- [5] K. Michaeli, N. Kantor-Uriel, R. Naaman, and D. H. Waldeck, "The electron's spin and molecular chirality - how are they related and how do they affect life processes?," *Chem. Soc. Rev.*, vol. 45, pp. 6478–6487, 2016.
- [6] R. Naaman, Y. Paltiel, and D. H. Waldeck, "Chiral molecules and the spin selectivity effect," *The Journal of Physical Chemistry Letters*, vol. 11, no. 9, pp. 3660–3666, 2020.
- [7] F. Evers, A. Aharony, N. Bar-Gill, O. Entin-Wohlman, P. Hedegard, O. Hod, P. Jelinek, G. Kamieniarz, M. Lemeshko, K. Michaeli, V. Mujica, R. Naaman, Y. Paltiel, S. Refaely-Abramson, O. Tal, J. Thijssen, M. Thoss, J. M. van Ruitenbeek, L. Venkataraman, D. H. Waldeck, B. Yan, and L. Kronik, "Theory of chirality induced spin selectivity: Progress and challenges," *Advanced Materials*, vol. 34, no. 13, p. 2106629, 2022.
- [8] R. Naaman and D. H. Waldeck, "Chiral-induced spin selectivity effect," *The Journal of Physical Chemistry Letters*, vol. 3, no. 16, pp. 2178–2187, 2012.
- [9] B. P. Bloom, B. M. Graff, S. Ghosh, D. N. Beratan, and D. H. Waldeck, "Chirality control of electron transfer in quantum dot assemblies," *Journal of the American Chemical Society*, vol. 139, no. 26, pp. 9038–9043, 2017.
- [10] P. C. Mondal, C. Fontanesi, D. H. Waldeck, and R. Naaman, "Spin-dependent transport through chiral molecules studied by spin-dependent electrochemistry," *Accounts of Chemical Research*, vol. 49, no. 11, pp. 2560–2568, 2016.
- [11] X. Yang, C. H. van der Wal, and B. J. van Wees, "Spin-dependent electron transmission model for chiral molecules in mesoscopic devices," *Phys. Rev. B*, vol. 99, p. 024418, 2019.
- [12] Z. Shang, T. Liu, Q. Yang, S. Cui, K. Xu, Y. Zhang, J. Deng, T. Zhai, and X. Wang, "Chiral-molecule-based spintronic devices," *Small*, vol. 18, no. 32, p. 2203015, 2022.
- [13] H. Al-Bustami, G. Koplovitz, D. Primc, S. Yochelis, E. Capua, D. Porath, R. Naaman, and Y. Paltiel, "Single nanoparticle magnetic spin memristor," *Small*, vol. 14, no. 30, p. 1801249, 2018.
- [14] C. Kulkarni, A. K. Mondal, T. K. Das, G. Grinbom,

- F. Tassinari, M. F. J. Mabesoone, E. W. Meijer, and R. Naaman, "Highly efficient and tunable filtering of electrons' spin by supramolecular chirality of nanofiber-based materials," *Advanced Materials*, vol. 32, no. 7, p. 1904965, 2020.
- [15] H. Min, J. E. Hill, N. A. Sinitsyn, B. R. Sahu, L. Kleinman, and A. H. MacDonald, "Intrinsic and rashba spin-orbit interactions in graphene sheets," *Phys. Rev. B*, vol. 74, p. 165310, 2006.
- [16] J. Fransson, "Charge redistribution and spin polarization driven by correlation induced electron exchange in chiral molecules," *Nano Letters*, vol. 21, pp. 3026–3032, 2021.
- [17] S. Mishra, A. K. Mondal, S. Pal, T. K. Das, E. Z. B. Smolinsky, G. Siligardi, and R. Naaman, "Length-dependent electron spin polarization in oligopeptides and dna," *The Journal of Physical Chemistry C*, vol. 124, no. 19, pp. 10776–10782, 2020.
- [18] M. Kettner, V. V. Maslyuk, D. Nurenberg, J. Seibel, R. Gutierrez, G. Cuniberti, K.-H. Ernst, and H. Zacharias, "Chirality-dependent electron spin filtering by molecular monolayers of helicenes," *The Journal of Physical Chemistry Letters*, vol. 9, no. 8, pp. 2025–2030, 2018.
- [19] J. Fransson, "Temperature activated chiral induced spin selectivity," *The Journal of Chemical Physics*, vol. 159, no. 8, p. 084115, 2023.
- [20] J. H. Bardarson, "A proof of the kramers degeneracy of transmission eigenvalues from antisymmetry of the scattering matrix," *Journal of Physics A: Mathematical and Theoretical*, vol. 41, p. 405203, sep 2008.
- [21] C. Vittmann, R. K. Kessing, J. Lim, S. F. Huelga, and M. B. Plenio, "Interface-induced conservation of momentum leads to chiral-induced spin selectivity," *The Journal of Physical Chemistry Letters*, vol. 13, no. 7, pp. 1791–1796, 2022.
- [22] X. Yang, C. H. van der Wal, and B. J. van Wees, "Detecting chirality in two-terminal electronic nanodevices," *Nano Letters*, vol. 20, no. 8, pp. 6148–6154, 2020.
- [23] S. Dalum and P. Hedegard, "Theory of chiral induced spin selectivity," *Nano Letters*, vol. 19, no. 8, pp. 5253–5259, 2019.
- [24] R. Gutierrez, E. Diaz, R. Naaman, and G. Cuniberti, "Spin-selective transport through helical molecular systems," *Phys. Rev. B*, vol. 85, p. 081404, 2012.
- [25] S. Yeganeh, M. A. Ratner, E. Medina, and V. Mujica, "Chiral electron transport: Scattering through helical potentials," *The Journal of Chemical Physics*, vol. 131, no. 1, p. 014707, 2009.
- [26] J. Fransson, "Chirality-induced spin selectivity: The role of electron correlations," *The Journal of Physical Chemistry Letters*, vol. 10, no. 22, pp. 7126–7132, 2019.
- [27] T. K. Das, F. Tassinari, R. Naaman, and J. Fransson, "Temperature-dependent chiral-induced spin selectivity effect: Experiments and theory," *The Journal of Physical Chemistry C*, vol. 126, no. 6, pp. 3257–3264, 2022.
- [28] E. Diaz, P. Albares, P. G. Estevez, J. M. Cervero, C. Gaul, E. Diez, and F. Dominguez-Adame, "Spin dynamics in helical molecules with nonlinear interactions," *New Journal of Physics*, vol. 20, no. 4, p. 043055, 2018.
- [29] J. Fransson, "Charge and spin dynamics and enantioselectivity in chiral molecules," *The Journal of Physical Chemistry Letters*, vol. 13, no. 3, pp. 808–814, 2022.
- [30] J. Fransson, "The chiral induced spin selectivity effect what it is, what it is not, and why it matters," *Israel Journal of Chemistry*, vol. 62, no. 11-12, p. e202200046, 2022.
- [31] A.-M. Guo and Q.-f. Sun, "Spin-selective transport of electrons in dna double helix," *Phys. Rev. Lett.*, vol. 108, p. 218102, 2012.
- [32] G.-F. Du, H.-H. Fu, and R. Wu, "Vibration-enhanced spin-selective transport of electrons in the dna double helix," *Phys. Rev. B*, vol. 102, p. 035431, 2020.
- [33] C. Lee, K.-H. Park, and M. Cho, "Vibrational dynamics of dna. i. vibrational basis modes and couplings," *The Journal of Chemical Physics*, vol. 125, no. 11, p. 114508, 2006.
- [34] A. A. Voityuk, J. Jortner, M. Bixon, and N. Rosch, "Electronic coupling between watson-crick pairs for hole transfer and transport in desoxyribonucleic acid," *The Journal of Chemical Physics*, vol. 114, no. 13, pp. 5614–5620, 2001.
- [35] K. Senthilkumar, F. C. Grozema, C. F. Guerra, F. M. Bickelhaupt, F. D. Lewis, Y. A. Berlin, M. A. Ratner, and L. D. A. Siebbeles, "Absolute rates of hole transfer in dna," *Journal of the American Chemical Society*, vol. 127, no. 42, pp. 14894–14903, 2005.
- [36] V. F. Kershaw and D. S. Kosov, "Nonequilibrium Green's function theory for nonadiabatic effects in quantum electron transport," *Journal of Chemical Physics*, vol. 147, no. 22, p. 224109, 2017.
- [37] V. F. Kershaw and D. S. Kosov, "Non-adiabatic corrections to electric current in molecular junctions due to nuclear motion at the molecule-electrode interfaces," *The Journal of Chemical Physics*, vol. 149, no. 4, p. 044121, 2018.
- [38] V. F. Kershaw and D. S. Kosov, "Non-equilibrium Green's function theory for non-adiabatic effects in quantum transport: Inclusion of electron-electron interactions," *Journal of Chemical Physics*, vol. 150, no. 7, p. 074101, 2019.
- [39] V. F. Kershaw and D. S. Kosov, "Non-adiabatic effects of nuclear motion in quantum transport of electrons: A self-consistent Keldysh–Langevin study," *The Journal of Chemical Physics*, vol. 153, no. 15, p. 154101, 2020.
- [40] B. Leimkuhler and C. Matthews, "Robust and efficient configurational molecular sampling via Langevin dynamics," *The Journal of Chemical Physics*, vol. 138, no. 17, p. 174102, 2013.
- [41] Y. Kim, H. Song, D. Kim, T. Lee, and H. Jeong, "Noise characteristics of charge tunneling via localized states in metal-molecule-metal junctions," *ACS Nano*, vol. 4, no. 8, pp. 4426–4430, 2010.
- [42] O. Adak, E. Rosenthal, J. Meisner, E. F. Andrade, A. N. Pasupathy, C. Nuckolls, M. S. Hybertsen, and L. Venkataraman, "Flicker noise as a probe of electronic interaction at metal-single molecule interfaces," *Nano Letters*, vol. 15, no. 6, pp. 4143–4149, 2015.
- [43] M. Galperin, A. Nitzan, and M. A. Ratner, "Inelastic tunneling effects on noise properties of molecular junctions," *Phys. Rev. B*, vol. 74, p. 075326, 2006.
- [44] D. Secker, S. Wagner, S. Ballmann, R. Härtle, M. Thoss, and H. B. Weber, "Resonant vibrations, peak broadening, and noise in single molecule contacts: The nature of the first conductance peak," *Phys. Rev. Lett.*, vol. 106, p. 136807, 2011.
- [45] M. Kumar, R. Avriller, A. L. Yeyati, and J. M. van Ruitenbeek, "Detection of vibration-mode scattering in electronic shot noise," *Phys. Rev. Lett.*, vol. 108,

- p. 146602, 2012.
- [46] C. Schinabeck, R. Härtle, H. B. Weber, and M. Thoss, “Current noise in single-molecule junctions induced by electronic-vibrational coupling,” *Phys. Rev. B*, vol. 90, p. 075409, 2014.
- [47] D. S. Kosov, “Non-renewal statistics for electron transport in a molecular junction with electron-vibration interaction,” *The Journal of Chemical Physics*, vol. 147, no. 10, p. 104109, 2017.
- [48] D. Djukic and J. M. van Ruitenbeek, “Shot noise measurements on a single molecule,” *Nano Letters*, vol. 6, no. 4, pp. 789–793, 2006.
- [49] P. J. Wheeler, J. N. Russom, K. Evans, N. S. King, and D. Natelson, “Shot noise suppression at room temperature in atomic-scale au junctions,” *Nano Letters*, vol. 10, no. 4, pp. 1287–1292, 2010.
- [50] M. Tsutsui, M. Taniguchi, and T. Kawai, “Single-molecule identification via electric current noise,” *Nat. Commun.*, vol. 1, p. 138, 2010.
- [51] D. Cho, H. Lee, S. Shekhar, M. Yang, J. Y. Park, and S. Hong, “Direct mapping of electrical noise sources in molecular wire-based devices,” *Scientific Reports*, vol. 7, p. 43411, 2017.
- [52] D. Xiang, T. Lee, Y. Kim, T. Mei, and Q. Wang, “Origin of discrete current fluctuations in a single molecule junction,” *Nanoscale*, vol. 6, pp. 13396–13401, 2014.
- [53] A. Burtzloff, A. Weismann, M. Brandbyge, and R. Berndt, “Shot noise as a probe of spin-polarized transport through single atoms,” *Phys. Rev. Lett.*, vol. 114, p. 016602, 2015.
- [54] P. Glasenapp, N. A. Sinitsyn, L. Yang, D. G. Rickel, D. Roy, A. Greilich, M. Bayer, and S. A. Crooker, “Spin noise spectroscopy beyond thermal equilibrium and linear response,” *Phys. Rev. Lett.*, vol. 113, p. 156601, 2014.
- [55] M. Oestreich, M. Römer, R. J. Haug, and D. Hägele, “Spin noise spectroscopy in gaas,” *Phys. Rev. Lett.*, vol. 95, p. 216603, 2005.
- [56] S. A. Crooker, D. G. Rickel, A. V. Balatsky, and D. L. Smith, “Spectroscopy of spontaneous spin noise as a probe of spin dynamics and magnetic resonance,” *Nature*, vol. 431, p. 49–52, 2004.
- [57] S. Mirzalian and A. Shokri, “Angular dependence of shot noise in the presence of rashba spin-orbit coupling in semiconductor spintronics junctions,” *Physica E: Low-dimensional Systems and Nanostructures*, vol. 54, pp. 59–64, 2013.
- [58] S. Pradhan and J. Fransson, “Shot noise as a probe of spin-correlated transport through single atoms,” *Phys. Rev. B*, vol. 97, p. 115409, 2018.
- [59] R. J. Preston, V. F. Kershaw, and D. S. Kosov, “Current-induced atomic motion, structural instabilities, and negative temperatures on molecule-electrode interfaces in electronic junctions,” *Phys. Rev. B*, vol. 101, p. 155415, 2020.